Int. J. Electrochem. Sci., 14 **(2019)** 8514 – 8531, doi: 10.20964/2019.09.16

International Journal of
ELECTROCHEMICAL
SCIENCE
www.electrochemsci.org

Application of a Novel PVA-based Proton Exchange Membrane Modified by Reactive Black KN-B for Low-temperature Fuel Cells

Tianchi Zhou[1,2,], Yang Li[2], Wei Wang[2], Lanhua He[2], Lu Cai[2], Chunmei Zeng[1]*

[1] Jiangsu R&D Center of the Ecological Dyes and Chemicals, Yancheng Polytechnic College, 285 Jie'fang South Road, Yancheng 224005, China
[2] College of Textile and Garment, YanCheng Institute of Technology, 1 Xi'wang middle Road, Yancheng 224051, China
[*]E-mail: 120413181@qq.com

Received: 1 May 2019 / *Accepted:* 18 June 2019 / *Published:* 31 July 2019

A novel proton-conducting membrane using poly(vinyl alcohol) (PVA) as matrix and Reactive Black KN-B as conductive component was fabricated through a solution casting method combined with a colour-fixing process. Fourier transform infrared (FT-IR) spectroscopy, X-ray photoelectron spectroscopy (XPS), X-ray diffraction (XRD) analysis and scanning electron microscopy (SEM) showed that KN-B dye was successfully grafted onto the PVA macromolecules and that the internal structure of the membrane became denser and rougher due to cross-linking of the colour-fixing agent DE. The H^+ conductivities of the synthesized membranes were evaluated using alternating current (AC) impedance measurements. The results indicated that the H^+ conductivity of PVA/KN-B membranes could reach 0.124 S cm^{-1} at 20 ℃. Thermal analysis and the investigation of mechanical properties, water uptake and swelling behaviour also showed that the membranes possessed excellent physical stability. When immersed in a solution of 30 wt.% hydrogen peroxide, PVA/KN-B/DE membranes showed excellent oxidative stability and their weights remained at approximately 72.8 wt.% of the original sample weight within 168 h at room temperature.

Keywords: Membrane; Proton conductivity; Vinyl-sulfone reactive dyes; Fuel cell; Oxidative stability

1. INTRODUCTION

Currently, the most common commercial proton exchange membrane (PEM) is Nafion® membrane which shows high ionic conductivity, low gas permeability, good electrochemical stability and chemical stability, but the high cost of production, potential fluorine pollution and difficult synthesis technology severely hinder its development [1]. Therefore, the development of new PEMs not only based on non-fluorinated materials but also having low cost and good electrochemical performance has

captured the attention of many researchers in recent years. Among various membrane matrixes, the fully aliphatic polymer PVA has been widely studied because it has many advantages such as excellent film-forming properties, good mechanical and physical performance, low cost, ease of modification and environmentally friendly characteristics [2]. Gomes [3] designed a novel PVA-based membrane doped with phosphotungstic acid and cross-linked by diethylenetriamine pentaacetic acid, the ionic conductivity of which reached the order of 10^{-3} S cm^{-1}. Alpay [4] prepared PVA/SPEEK/TEOS tri-component blend membranes that showed excellent conductivity of 8.5×10^{-2} S/cm at 80 ℃ and exhibited higher cell performance compared with that of Nafion® 117. González [5] fabricated a kind of composite PVA-based membrane modified by sulfosuccinic acid (SSA) and graphene oxide (GO), and the maximum value of conductivity reached 3.06×10^{-3} S/cm at 30 ℃. Although research on PVA-based proton membranes has made significant progress, current research in this field still has some deficiencies, one of which is weak interactions among the matrix, conductive component and additives which must be addressed to enhance application performance.

KN-type reactive dyes are always used to dye cotton fibre at moderate temperature (approximately 60 ℃) and contain reactive vinyl sulfone groups that bond covalently to cellulose through nucleophilic addition reaction as well as sulfonic groups to enhance the water solubility [6]. In this work, the reactive dye KN-B (Figure 1a) was chosen as a charge carrier to blend with PVA to form a novel proton exchange membrane. PVA contains a large amount of hydroxyl groups and can lose hydrogen ions under alkaline conditions; thus generated PVA-O^- ions may attack the carbonium ion intermediates of vinyl sulfone groups to form covalent bonds, as displayed in Figure 1b. KN-B can not only graft onto the PVA macromolecular structure but also react with different PVA macromolecules to form cross-linking, which can enhance the inner structure of the membrane and improve the mechanical properties. Furthermore, the formed covalent bond between KN-type reactive dyes and PVA possess excellent chemical stability under acidic conditions [7], which establishes a foundation for its application in PEM fuel cells. As both the base material PVA and charge carrier KN-B have good hydrophilicity, water uptake by the membrane should be carefully adjusted to avoid excessive swelling and improve mechanical performance. In our previous work [8-11], glutaraldehyde (GA) was adopted to perform a chemical cross-linking process for the PVA matrix, but the cross-linking density of the membrane was difficult to control, and aldehydes are not friendly to the environment and health [12]. Containing two active epoxy groups, the colour-fixing agent DE (Figure 1c) can undergo etherification with PVA and play a vital role in constructing and adjusting the cross-linking structure of the membrane. Moreover, the quaternary ammonium cationic groups of DE can effectively absorb more anionic KN-B molecules and improve the conductivity performance of the membrane.

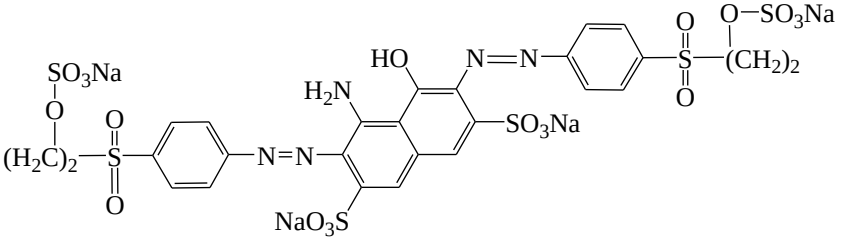

(a)

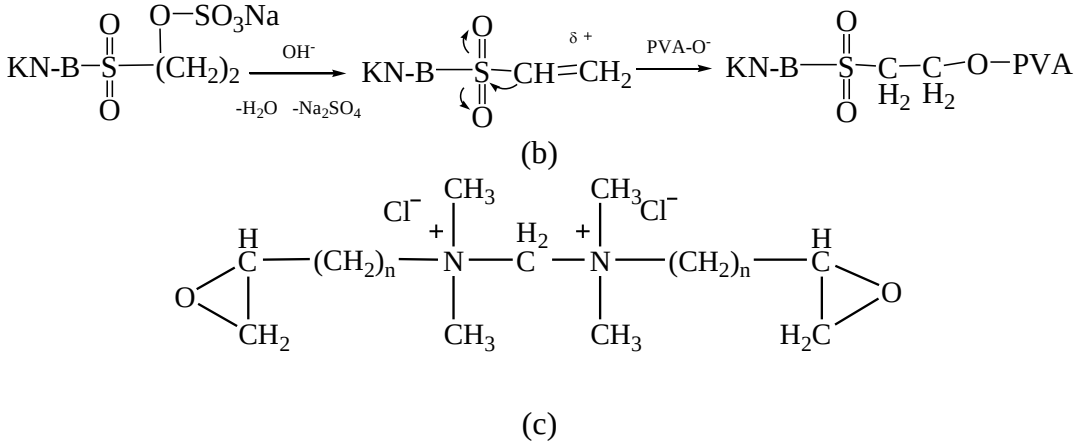

Figure 1. The chemical structure of KN-B (a), the chemical reaction between KN-B and PVA (b) and the chemical structure of DE (c).

Based on the above concept, we fabricated a new PEM by using dyeing and fixing method to achieve the goal of improving the mechanical properties, ionic conductivity and durable life of the membrane. This dyeing and modification method of introducing sulfonic groups into PVA is superior to traditional methods such as the sulfonation process with sulfonic reagents which may lead to more byproducts and a decrease in conductivity [13]; grafting methods by radiation which may result in the obvious deterioration of polymer structure [14]; and chemical modification methods in harsh conditions or using expensive chemical agents [15,16]. Using FT-IR, SEM, XRD and XPS, the chemical structure and microstructure of the prepared membranes were comprehensively analysed. Thermogravimetric (TG) analysis, mechanical stretching and weight loss experiments using H_2O_2 were also adopted to determine the membranes' thermal, mechanical and chemical stability respectively. To evaluate the application performance in acidic fuel cells, the H^+ conductivity (σ), ion exchange capacity (IEC) and relative water content (i.e., water uptake, WU) were also addressed.

2. EXPERIMENTAL

2.1 Purification of the reactive dye KN-B

First, 8 g of the reactive dye KN-B (Wujiang Taoyuan Dyestuff Co.,Ltd, China) was placed in a beaker and dissolved in 60 mL N,N-dimethylformamide (DMF) (Sinopharm Chemical Reagent Co.,Ltd, China) by a magnetic stirrer. Second, vacuum filtration was carried out to remove salts of the KN-type reactive dye and the filtered liquid was obtained after using 5 mL DMF to wash the cake several times. Subsequently a reduced-pressure distillation by a rotary evaporator was performed to concentrate the filtered liquid. Third, 100 mL anhydrous diethyl ether (Sinopharm Chemical Reagent Co.,Ltd, China) was added to the solution to extract the DMF and the dye settled out after the solution was placed in a freezer at -5 ℃ for 15 min. After vacuum filtration and washing several times with anhydrous diethyl ether, the purified KN-B was obtained by vacuum drying.

2.2 Membrane preparation

A PVA water solution was obtained by dissolving PVA (formula weight 86,000-89,000, alcoholysis degree 99%, Aldrich) in pure water at 90 ℃ for 4 h, and then its pH was adjusted to 10 with 1 M NaOH solution. According to the ratio of PVA:KN-B by mass (1:0.5), purified KN-B was dissolved in a small amount of deionized water. Subsequently, a homogeneous solution was obtained by adding the dyeing liquid dropwise into the PVA solution under sufficient stirring for 3 h at room temperature. After being heated to 70 ℃, the mixed solution was continuously stirred at this temperature for 1 h. Then, the cooled solution was degassed under vacuum, followed by casting the solution into plastic dishes and natural drying them under ambient conditions. After being removed from the dishes, the membranes were soaked in a fixing finishing liquid (5 g/L DE, bath ratio 1:50) for 30 min at 40 ℃. Subsequently, the membranes were dried at 160 ℃ for 10 min to induce thermal and chemical cross-linking reactions, followed by sufficient washing. Owing to the cross-linking effect, a three-dimensional network structure was constructed and the KN-B component was better retained in the membranes. Before the membranes were used, they were soaked in 0.5 M H_2SO_4 solutions for 24 h to replace Na^+ with H^+, and then these membranes were rinsed with distilled water until the pH of the membranes' surface reached neutral. Finally, the prepared membranes with thicknesses of 70-90 μm were sealed in polyethylene bags and set aside. The inner structure of the PVA/KN-B/DE membrane is shown in Figure 2.

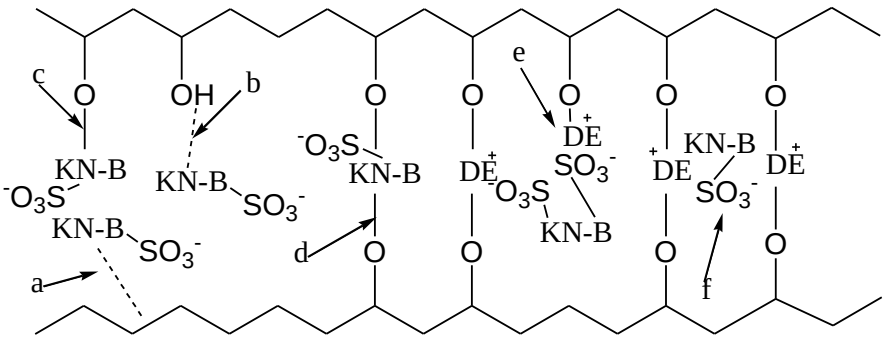

Figure 2. Inner structure of PVA/KN-B/DE membrane. a. Van der Wa als forces, b. hydrogen bonds, c. grafting, d. cross-linking, e. electrostatic forces, f. trapping.

2.3 Membrane characterizations

With the help of an attenuated total reflectance instrument, FT-IR spectroscopy (Tensor27, Bucker) was adopted to analyse the structural properties of the membrane. The analysis was carried out with a scan range of 4000–600 cm^{-1} and a resolution of 4 cm^{-1}.

The morphology of the membrane was analysed by using an FEI Sirion 200 field-emission SEM (JSM-5600LV, JEOL) at 5 kV. Before collecting the SEM images, each of the membrane samples was sputtered with an ultra-thin coating of electrically conducting gold metal to facilitate or improve the imaging of the sample. Then, the cross-section morphology, magnified 10,000 times, was observed carefully.

Using a TG 209 analyser (Netzsch, Germany) at a heating rate of 10 °C min^{-1} up to 800 °C in N_2 atmosphere, TG analysis was performed to investigate the thermal stability of the prepared film. The vacant alumina pan was employed as a reference throughout the experiment.

Under the conditions of room temperature, a 12 mm/min drawing rate and 60% relative humidity, mechanical tests were carried out by using a H5K-S stretch testing instrument (Hounsfield, England). By averaging the values from five sample strips with standard dimensions of 1×5 cm, the tensile strength, elongation at break and Young's modulus of the membrane were obtained.

2.4 Water uptake and Swelling ratio

Water uptake is often used to evaluate the swelling behaviour of a membrane and can be calculated from the mass change of a fully hydrated membrane before and after complete drying. Under ambient conditions, a dry membrane was immersed in deionized water for 24 h to allow complete swelling. Then, a filter paper was used to carefully wipe off the surface water, after which the hydrated membrane was weighed at once. Finally, the membrane was dried in a vacuum oven at 105 ℃ for 4 h. The water uptake (*WU*) of the membrane was calculated according to the following formula:

$$WU = (W_{wet} - W_{dry})/W_{dry} \quad (1)$$

where W_{wet} is the mass of the fully hydrated membrane and W_{dry} is the mass of the completely dry membrane.

The swelling ratio can be determined by the dimension change of the membrane. First, the membrane was heat treated at 105 °C for 1 h and its thickness (T_{dry}) and surface area (A_{dry}) were measured immediately. Then the dry membrane was allowed to stand in deionized water under ambient conditions for 24 h. After that, the immersed membrane was removed and wiped carefully with a filter paper for surface water removal. Subsequently, the membrane thickness (T_{wet}) and surface area (A_{wet}) were investigated immediately.

$$\text{Thickness swelling (\%)} = (T_{wet} - T_{dry})/T_{dry} \quad (2)$$

$$\text{Plane swelling (\%)} = (A_{wet} - A_{dry})/A_{dry} \quad (3)$$

2.5 H^+ conductivity and ion exchange capacity

The measurement of H^+ conductivity was performed by using a CHI760 electrochemical impedance analyser (Shanghai Chenhua, China) to explore the electrochemical AC impedance. Impedance spectroscopy in three-electrode mode was carried out in an AC frequency range from 100 kHz to 0.1 Hz at an oscillating voltage of 100 mV. After being sufficiently hydrated, the membrane was clamped in a polytetrafluoroethylene conductivity cell with platinum strips attached to provide electrical contacts [17]. Then, the cell was placed in a temperature-controlled chamber, and the measurements were performed within a temperature range from 20 ℃ to 80 ℃. The membranes were in contact with water throughout the measurements. The H^+ conductivity of the membrane was calculated by the following formula:

$$\sigma = l / (RTW) \quad (4)$$

where σ denotes the proton conductivity of the membrane, *R* represents the resistance (ohm) of the membrane, *l* is the fixed distance (cm) between the two platinum strips, and *T* and *W* refer to the thickness (cm) and width (cm) of the membrane, respectively.

To determine the proton conductivity mechanism, the IEC provides highly important information about how many active groups exist in the membrane. Chemical titration was carried out to determine the IEC value of the membrane. The synthesized dry membrane was first weighed and then immersed in 30 mL of 2 M NaCl aqueous solution for 2 days at room temperature to completely replace H^+ ions in the membrane with Na^+ ions. Subsequently, 0.01 M NaOH solution was used to titrate the obtained acidic solution. The amount of titrant used for the membrane was recorded and the IEC value was obtained by using the following formula:

$$IEC\ (meq/g) = V_{Consumed\ NaOH} \times C_{Molarity\ of\ NaOH}/W_{dry} \quad (5)$$

where $V_{Consumed\ NaOH}$ is the volume of NaOH solution neutralized by the acidic solution and $C_{Molarity\ of\ NaOH}$ represents the molar concentration of the NaOH solution.

2.6 Oxidative stability

An experiment measuring weight loss of the membrane over the time was carried out to investigate the oxidative stability of the synthesized membrane. The membrane that needed to be measured was soaked in H_2O_2 (30 wt.%) solution at room temperature for a period of time.

3. RESULTS AND DISCUSSION

3.1 FT-IR studies

The infrared spectra of the pristine PVA membrane, the PVA/KN-B membrane and the PVA/KN-B/DE membrane are shown in Figure 3. The peaks between 3250 cm^{-1} and 3400 cm^{-1} are mainly ascribed to the stretching vibration of N-H and O-H bonds. The absorption peaks between 2850 cm^{-1} and 2950 cm^{-1} are caused by the stretching of -CH_2- and -CH_3 groups. The peak at 2850 cm^{-1} from the PVA/KN-B/DE membrane obviously lags behind those of the other two and this peak may be due to -CH_3 groups from DE rather than PVA and KN-B. This result was observed because the PVA/KN-B/DE membrane contains -CH_3 groups in addition to -CH_2- groups while the pristine PVA membrane and the PVA/KN-B membrane only contain -CH_2- groups. The peak at 1374 cm^{-1} of the PVA/KN-B/DE membrane is further evidence of the bending vibration of -CH_3 groups, whereas the peak at 1480 cm^{-1} is revealed as the specific signal of C-N vibration in DE. The peak at 1593 cm^{-1} of PVA/KN-B and the peak at 1600 cm^{-1} of PVA/KN-B/DE may be caused by N=N bonds. The peaks at 1292 cm^{-1}, 1180 cm^{-1} and 1045 cm^{-1} from PVA/KN-B and the peaks at 1289 cm^{-1}, 1176 cm^{-1} and 1043 cm^{-1} from PVA/KN-B/DE may be due to sulfuryl groups and sulfonic groups of KN-B. The peaks at 1129 cm^{-1} and 1091 cm^{-1} from PVA/KN-B and 1124 cm^{-1} and 1092 cm^{-1} from PVA/KN-B/DE might arise from C-O-C and C-O bonds, which demonstrates that the chemical reaction between PVA and KN-B, and the cross-linking reaction between PVA and DE successfully occur. These results show that KN-B and DE were successfully

introduced into the PVA matrix, which might not only bring sulfonic groups into the membrane matrix to improve electrical conductivity but also construct three-dimensional network structure to optimize the mechanical performance.

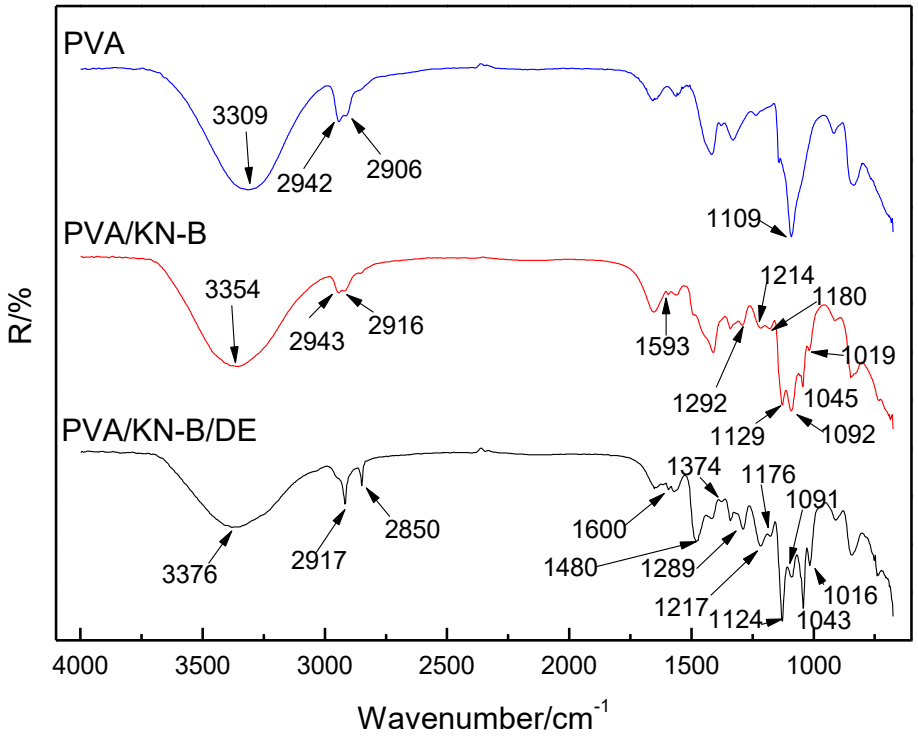

Figure 3. Infrared spectra of the pristine PVA membrane, the PVA/KN-B membrane and the PVA/KN-B/DE membrane.

3.2 Membrane morphology

Cross-section SEM images of the pristine PVA membrane, the PVA/KN-B membrane and the PVA/KN-B/DE membrane are presented in Figure 4. From Figure 4a and Figure 4b, we can see that the cross section of the pristine PVA membrane is relatively smooth and homogeneous. However, after blending with KN-B, the cross section shows some roughness, and some very small particles are irregularly embedded in the film. Even so, the PVA/KN-B membrane maintains a relatively continuous phase and does not show serious phase separation phenomena. This may be because the majority of KN-B can be absorbed and grafted firmly onto the PVA matrix in small molecular form during the process of blending while a small quantity of dye aggregates. From Figure.4c, it can be observed that many micro particles are distributed evenly throughout the membrane, and this phenomenon may be caused by the aggregation of dye molecules. DE contains quaternary ammonium cationic groups that can absorb surrounding anionic dyes by electrostatic attraction. Furthermore, baking treatment exacerbates aggregation due to the rapid evaporation of water. DE can not only build bridges between the dye and the PVA matrix but also form a network structure that can firmly clamp dye aggregates in the membrane to avoid the loss of unreacted and poorly absorbed dyes.

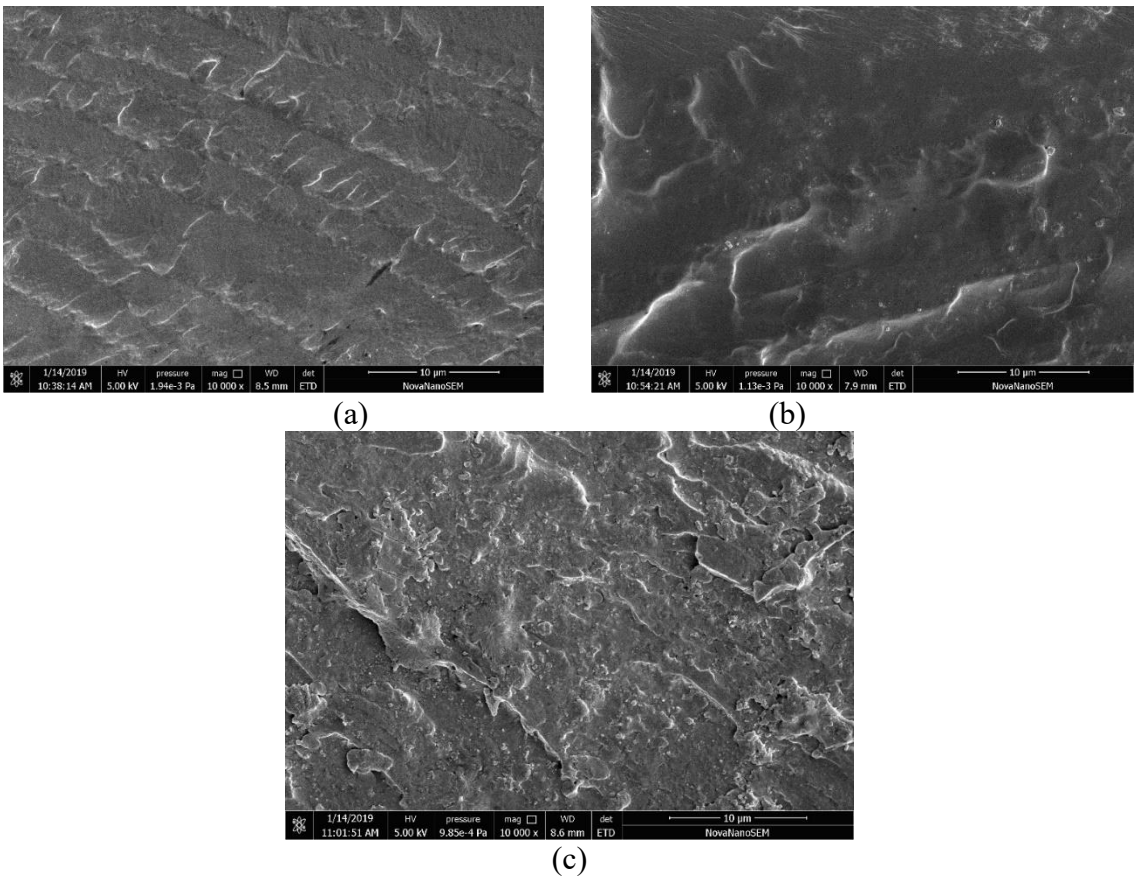

Figure 4. Cross-section SEM morphologies of the PVA membrane (a), the PVA/KN-B membrane (b) and the PVA/KN-B/DE membrane (c).

3.3 Thermal analysis

The thermal stabilities of the pristine PVA membrane, the PVA/KN-B membrane and the PVA/KN-B/DE membrane were evaluated using a thermogravimetric analysis and differential scanning calorimeter. From Figure 5A and Figure 5B, the stages of weight loss, at approximately 30 - 200 ℃, 200 - 360 ℃ and 360 - 520 ℃, can be observed clearly in all three curves. The first stage may be due to the evaporation of water from the film or the moisture absorbed from the atmosphere. The second stage may arise from the cleavage of -SO_3H groups [18], the breaking of cross-linking bridges between DE and PVA, the decomposition of DE and KN-B, and even the destruction of part of the PVA backbones. The third stage mainly results from the breaking and degradation of PVA backbones [19]. The characteristic data of the TGA curves (char yield, $T_{-50\%}$, $T_{2\text{-onset}}$ and T_{max}) are shown in Table 1. $T_{2\text{-onset}}$ represents the initial degradation temperature of stage 2, $T_{-50\%}$ represents the temperature of 50% weight loss and T_{max} represents the temperature of the maximum degradation rate during the heating process.

As shown in Table 1, the $T_{2\text{-onset}}$ of the PVA membrane is 175 ℃, but after modification by dyeing and cross-linking, the value increases to 195 ℃ and 205 ℃, respectively. $T_{2\text{-onset}}$ improves significantly after dyeing with KN-B and is further improved through the combination of dyeing and cross-linking treatment. This may be caused by the hydrogen bonding and slight cross-linking formed between PVA and KN-B and the further cross-linking effect provided by DE. The PVA/KN-B/DE membrane shows

high thermal stability up to 210 ℃, indicating that the designed film has sufficient thermal stability to support the normal operation of a fuel cell at 100 ℃. From Table 1, the T_{max} values of the three membranes are 261 ℃, 271 ℃ and 291 ℃, while the $T_{-50\%}$ values are 282 ℃, 288 ℃, and 400 ℃. All these data show an ascending trend, indicating that with further processing steps, the thermal stability of the membrane is enhanced This conclusion can be further confirmed by the tendency of the TG curves, where the curve of the pristine PVA is steeper than those of the other membranes. The increased shallowness of the curve indicates that heat release is significantly inhibited after modification. Moreover, the ultimate char yields of the pristine PVA membrane, the PVA/KN-B membrane and the PVA/KN-B/DE membrane are 9.57%, 17.87% and 14.14%, also indicating that the modified membranes possess higher thermal stability than the pristine PVA membrane.

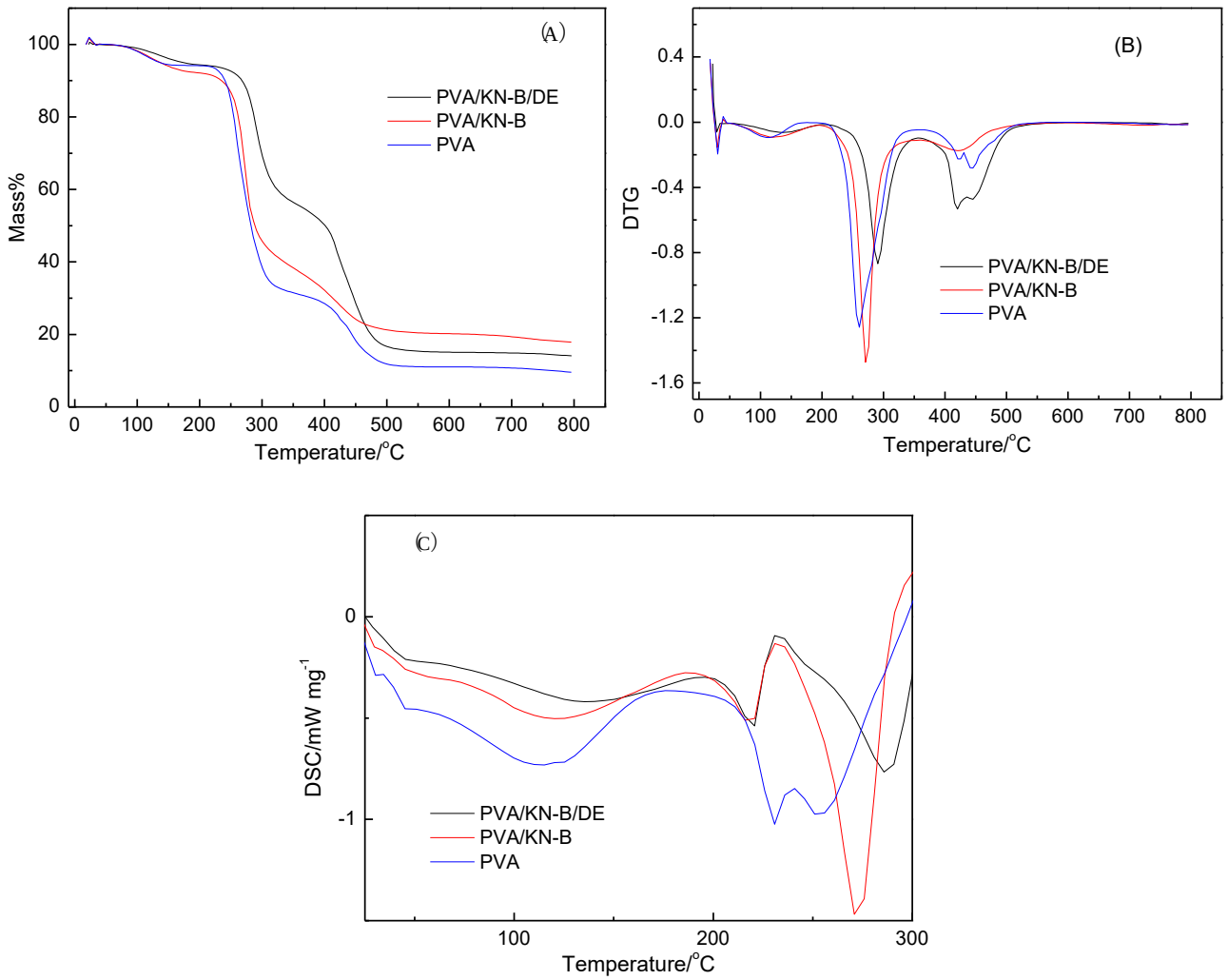

Figure 5. Thermal stabilities of the prepared membranes.(A)TG, (B)DTG, (C)DSC.

Figure 5C shows DSC plots, which are usually used to understand the thermal behaviour of polymers, especially to find the Tg (glass transition temperature) of polymers [20]. Based on temperatures ranging from 50 -150 ℃, the Tg of the PVA membrane is 81.3 ℃, which is also in

agreement with the Tg value (80.15 ℃) of pure PVA reported by Liew [22]. After modification by KN-B and DE, the value increases to 91.6 ℃ (PVA/KN-B) and 97.4 ℃ (PVA/KN-B/DE), suggesting that the thermal stability of the membrane increases because of the presence of hydrogen-bonding and cross-linking effects. The DSC scan also shows two endothermic peaks between 200 ℃ and 300 ℃. The former may be caused by melting behaviour and the latter may correspond to the pyrolytic endothermic membrane degradation reactions. Compared to the pristine PVA membrane, the PVA/KN-B/DE membrane shows not only a smaller intensity but also a later temperature range, which indicates that the thermal stability of the film is significantly improved.

Table 1. TGA data for the PVA membrane, the PVA/KN-B membrane and the PVA/KN-B/DE membrane

Membrane	$T_{2\text{-onset}}$ (℃)	T_{max} (℃)	$T_{50\%}$	Char yield (%)
Pristine PVA membrane	175	261	282	9.57%
PVA/KN-B membrane	195	271	288	17.87%
PVA/KN-B/DE membrane	205	291	400	14.14%

3.4 XRD analysis

X-ray diffraction analysis was performed to determine the change in the crystallinity of the pristine PVA membrane, the PVA/KN-B membrane and the PVA/KN-B/DE membrane. As shown in Figure 6, all the curves show two major peaks. The peak located near $2\theta = 20.2° \pm 0.2$ is due to the semi-crystalline nature of PVA [22] and corresponds to an orthorhombic lattice (110) reflection [23]. The peak at $23.3° \pm 0.3$ may arise from the lattice plane (200) of the crystalline regions in these PVA-based membranes [24]. Compared to the peaks for the PVA membrane, the peaks of the PVA/KN-B membrane and the PVA/KN-B/DE membrane show a slight left-shift, which is attributed to doping and chemical reaction effects. Furthermore, there is an obvious increase in the intensity of the peak at $20.2°\pm0.2$ after the DE treatment process, indicating an increase in the percentage of crystallinity of the samples due to the cross-linking reaction. By comparison with the PVA membrane, it could be observed that a new peak appeared at approximately 16.5° in the PVA/KN-B/DE membrane, which might be caused by dye aggregation, as discussed in the SEM analysis section.

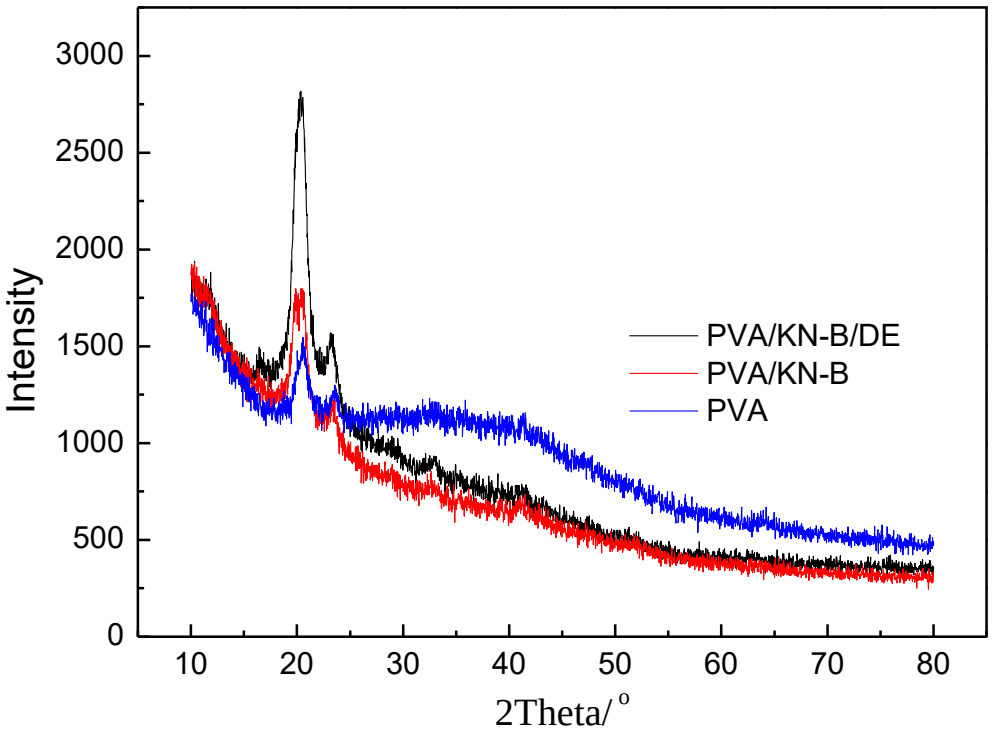

Figure 6. The X-ray diffraction patterns of the pristine PVA membrane, the PVA/KN-B membrane and the PVA/KN-B/DE membrane.

3.5 XPS analysis

To further investigate the chemical composition of the prepared membrane, XPS analysis was performed for the elements of carbon, nitrogen, oxygen and sulfur on the membrane surface. As Figure 7a illustrates, the spectrum of PVA mainly contains C (C1s, 284.78 eV) and O (O1s, 531.46 eV) elements. The spectrum of PVA/KN-B mainly contains C (C1s, 284.80 eV), O (O1s, 531.73 eV), N (N1s, 399.68 eV) and S (S2p, 168.21 eV), and the spectrum of PVA/KN-B/DE mainly contains C (C1s, 284.8 eV), O (O1s, 532.17 eV), N (N1s, 402.36 eV) and S (S2p, 167.72 eV). All the photoelectron peak positions are in accordance with the reported literature [25-27]. Obviously, the S2p peak and N1s peak of the PVA/KN-B membrane and the PVA/KN-B/DE membrane, which are different from the peaks in the XPS spectrum of the PVA membrane, are due to the incorporation of KN-B and DE into the membrane, indicating that dyeing and cross-linking were successfully performed. The deconvoluted C1s XPS spectrum of PVA/KN-B/DE is shown in Figure 7b. The peak with a binding energy (BE) of 288.79 eV represents C–S species [28], while the peak component with a BE at 285.23 eV is attributed to C-N [29], which is evidence of the existence of KN-B and DE. The component peak at 286.25 eV is assigned to C-O [30], and that at 284.78 eV arises from C=C/C-C [25], whereas the peak at 284.39 eV is attributed to C-H [27].

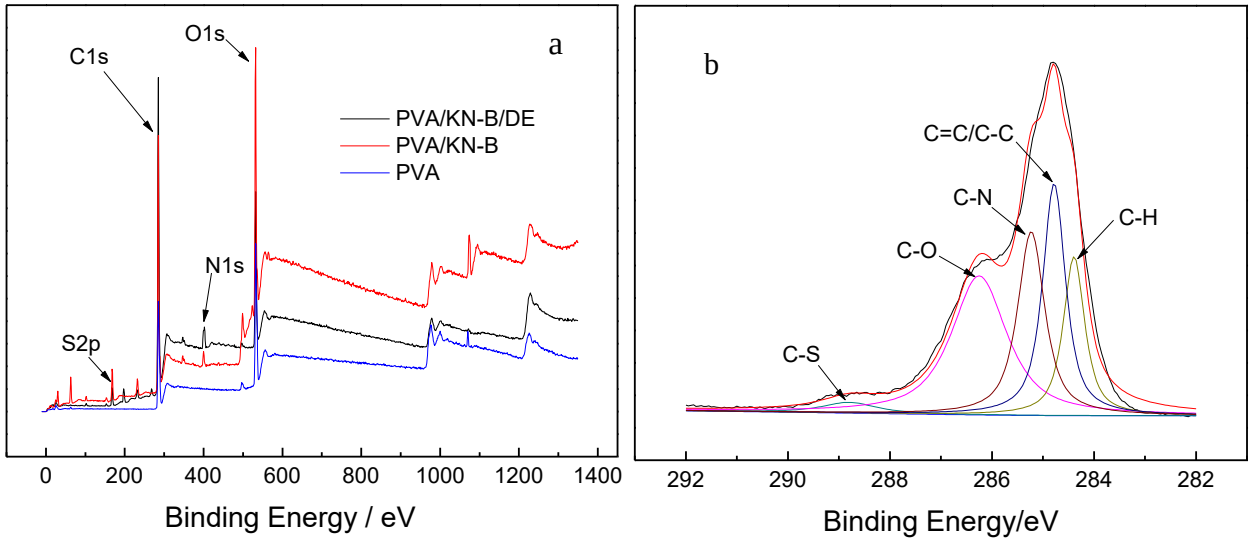

Figure 7. XPS analysis: (a) full spectra, and (b) spectrum of C1s.

3.6 Mechanical properties

In this study, the mechanical properties, including tensile strength, elongation at break and Young's modulus, of the prepared membranes were investigated and the results of the typical stress-strain curves are summarized in Figure 8. All of the prepared membranes first show elastic deformation, then present plastic deformation after reaching the yield point, and eventually break. The average tensile strengths of the pristine PVA membranes, the PVA/KN-B membranes and the PVA/KN-B/DE membranes are 24.1 MPa, 31.3 MPa and 55.6 MPa, respectively. The corresponding elongations at break are 197.9%, 172.4% and 161.2%, whereas the Young's moduli are 393.3 MPa, 114.3 MPa and 1766.6 MPa, respectively. In terms of tensile strength and Young's modulus, the PVA/KN-B/DE membranes show a remarkable improvement in material rigidity compared to the pristine PVA membranes, which can be attributed to the enhanced hydrogen-bond interactions among different polar groups from KN-B and PVA molecular chains and the enhanced compact and dense structure due to the cross-linking effect brought about by DE. However, the average elongation at break of the PVA/KN-B/DE membranes is decreased compared with that of the pristine PVA membranes, indicating a decrease in flexibility and toughness after dyeing and cross-linking. Despite the decrease in elongation at break, the PVA/KN-B/DE membrane still has good elongation up to 161.2%, indicating that the membrane still has excellent flexibility and toughness. The tensile strength is higher than that of PVA/QHECE membranes (29.6 MPa) [9], QBAPB/PVA membranes (18.3 MPa) [31] and PVA/PDDA membranes (15.3 MPa) [11] and is close to that of Nafion® 115 (43 MPa) [32], PVDF/PVA membranes (36.8 MPa) [33] and PVA-Alg membranes [34] (38.5 MPa). Thus, this kind of membrane has excellent prospects since the film could withstand the pressure exerted during the membrane electrode assembly (MEA) preparation process.

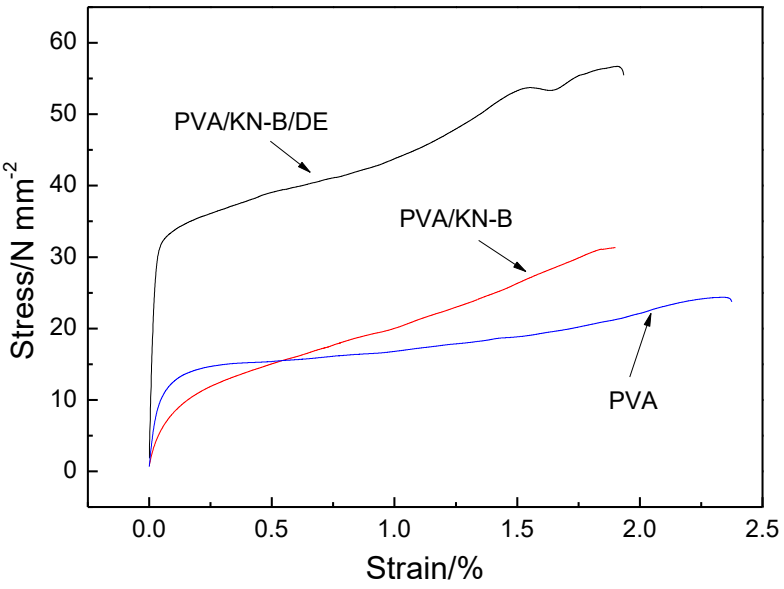

Figure 8. Stress-strain curves of the prepared membranes.

3.7 Water uptake (WU) and H^+ conductivity

The Grotthuss mechanism and vehicle mechanism are the two most important mechanisms to explain the diffusion and transportation of H^+ in proton membrane fuel cells. In the two mechanisms, water plays a vital role in the movement of ions. Although an appropriate increase in water content will increase the ionic conductivity of the membrane because ionic transport channels can be formed effectively, too much water will have a dilution effect on the H^+ concentration, which brings down the conductivity accordingly. Furthermore, too much water can decrease the dimensional stability of the membrane, which increases the membrane's fragility and results in high permeability [18,35]. Regarding the swelling ratio (SR), severe swelling behaviour in the plane direction may result in poor adhesion between the catalyst layer and membrane surface or may reduce the contact surface area in MEA, while swelling in the thickness direction may increase the resistance to proton diffusion through the membrane [36]. Therefore, WU and SR are important parameters worthy of study. The WU and SR data in Figure 9 show a significant decrease after the cross-linking process with DE. This may arise from the reaction of DE with unconsumed hydroxyl groups in PVA; such reaction forms a more compact inner structure and reduces the number of free voids containing water molecules [37]. This structure can be confirmed by SEM analysis and FT-IR spectra and is also supported by the values of elongation at break and tensile strength as shown in section 3.6. Taken together, the decreased WU and SR of the membranes are desirable for fuel cell applications.

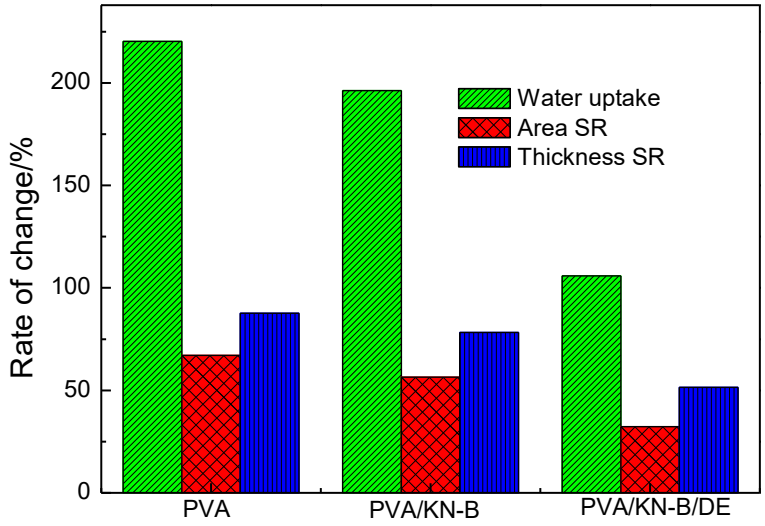

Figure 9. Water uptake and swelling ratios of the prepared membranes.

For PEM performance in fuel cell applications, H^+ conductivity is one of the most important indicators because a high proton conductivity value always indicates good proton exchange properties. Moreover, the change in H^+ conductivity at different temperatures can reveal the ionic conducting mechanism. As shown in Figure 10, the proton conductivities of the PVA/KN-B membranes and the PVA/KN-B/DE membranes at different temperatures were investigated. The membranes were fully hydrated during the measurement process and the effect of humidification was eliminated. The membranes' proton conductivity values tend to increase with increasing temperature from 20 ℃ to 80 ℃. This result can be interpreted in terms of three aspects: high temperature favours the mobility of H^+ in the membrane; high temperature provides more free space in the film, which benefits the transport of ions [38]; and high temperature can lower the voltage loss during the use process of fuel cells and facilitate the response rate of the electro chemical reactions. Average H^+ conductivities of 1.24×10^{-1} S cm^{-1} and 1.03×10^{-1} S cm^{-1} at 20 ℃ were reached for the PVA/KN-B membranes and the PVA/KN-B/DE membranes, which exceed the H^+ conductivity of Nafion® 212 (9.72×10^{-2} S cm^{-1} at 20 ℃) measured under the same conditions [39]. The average H^+ conductivities of the PVA/KN-B membranes and the PVA/KN-B/DE membranes reached 1.77×10^{-1} S cm^{-1} and 1.54×10^{-1} S cm^{-1} at 80 ℃, respectively, indicating that this type of membrane has excellent conductive performance. The proton conductivity values are higher than those of PVA/SSA/GO membranes (3.06×10^{-3} S cm^{-1} at 30 ℃) [5], SPES/$STiO_2$–PANI membranes (2.30×10^{-4} S cm^{-1} at room temperature) [40] and PES/SPEEK/TiO_2 membranes (4.57×10^{-4} S cm^{-1} at room temperature) [41], and are close to those of sulfonated poly(arylene ether sulfone)/graphene oxide membranes (1.31×10^{-1} S cm^{-1} at 80 ℃) [42], PVA/SPEEK/TEOS tri-component blend membranes (8.5×10^{-2} S/cm at 80 ℃) [4], Nafion-sulfonated silica composite membranes (over 2×10^{-1} S cm^{-1} at 80 ℃) [43], Nafion phosphonic acid composite membranes (8.73×10^{-2} S cm^{-1} at 60 ℃) [44], (PVDF-g-PSSA)/SGO@SiO_2 membranes (7.8×10^{-2} S/cm at room temperature) [45] and SPEES-SA/SMZ membranes (1.24×10^{-1} S cm^{-1} at 80 ℃) [46]. Compared with these membranes, the PVA/KN-B/DE membrane has the advantages of ease of preparation, low manufacturing cost, and stable and good performance and has good application prospects.

The relationship between H^+ conductivity and temperature for proton exchange membrane fuel cells can be expressed by the Arrhenius equation which has been described in detail in our previous work [47]. Based on the analysis principle of linear regression, the values of *-Ea/R* provided by the slope of the Arrhenius plot are 0.661 and 0.792; thus, the calculated values of *Ea* are 5.49 kJ mol^{-1} and 6.58 kJ mol^{-1}, indicating that both the mechanisms for the transfer of ions (Grotthuss mechanism and vehicle mechanism) through the film co-exist in the conductive process, but the Grotthuss mechanism plays a dominant role [48]. From the data listed in Figure 10, the PVA/KN-B membranes exhibit higher conductive values than the PVA/KN-B/DE membranes. This can be explained by the fact that the former has a larger number of ionic exchange groups than the latter, which is confirmed by the average IEC values of the PVA/KN-B membranes (0.94 meq/g) and the PVA/KN-B/DE membranes (0.81 meq/g). The cross-linked structure may prevent the additional penetration of protons into the bulk of the membrane and narrow the proton transfer channels in the membrane [49].

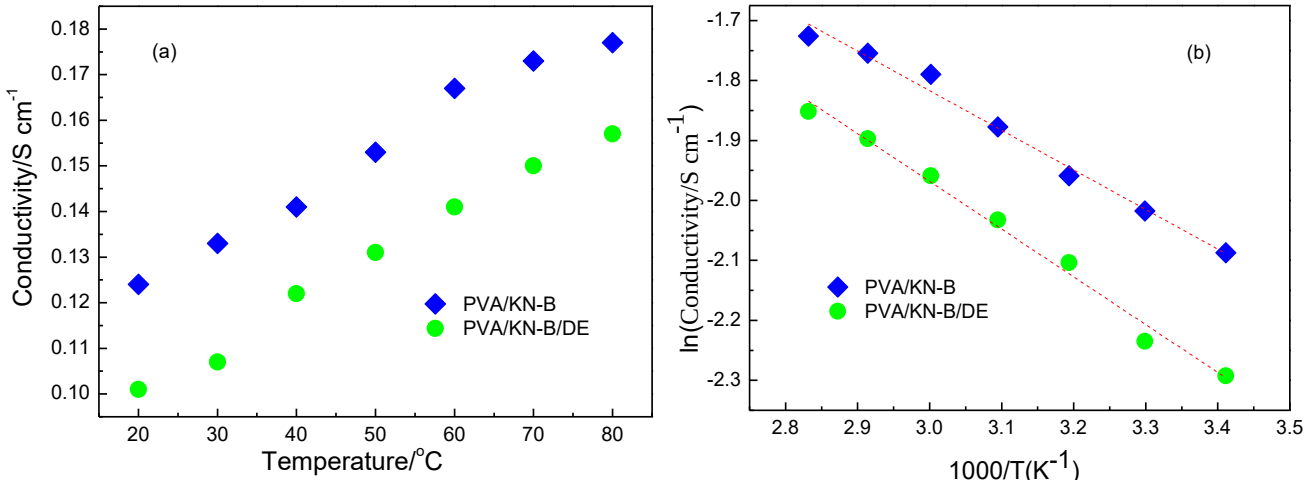

Figure 10. Temperature dependence of the proton conductivity of PVA/KN-B membranes and PVA/KN-B/DE membranes in the range of 20 - 80 ℃.

3.8 Oxidative stability

At the anode side of fuel cells, a complex oxygen reduction reaction that results in the generation of radicals such as HO· and HOO· might occur. These radicals may react with PVA macromolecules and cause breakage and degradation of the polymer backbone; subsequently, the application performance shows a sharp decline [50]. Thus, the oxidative stability of films is a critical issue that should attract considerable attention. The oxidative stabilities of the synthesized membranes were evaluated by immersing the membranes in H_2O_2 (30 wt.%) solution and measuring the weight loss at regular intervals at room temperature. As shown in Figure 11, the synthesized membranes undergo an obvious decrease in weight loss at first, and then the loss levels off gradually. Finally, the average weight loss of the PVA/KN-B membranes was determined to be 52.1 wt.% of the original sample weight via a continuous test that lasted for 168 hours at room temperature, while that of the PVA/KN-B/DE membranes was 27.2 wt.%. This indicates that cross-linked membranes have better oxidative longevity than membranes

without DE cross-linking, which is mainly due to the protective effect of the cross-linked network structure and the effective consumption of radicals by the dye. The PVA/KN-B/DE membrane shows better oxidative stability than that of some hydrocarbon films with aromatic or carbohydrate skeletons reported recently in the literature [51-54]; the previously reported membranes showed significant dissolution after being soaked in Fenton 's reagent solution, or degraded obviously in H_2O_2 (30 wt.%), or were even easily damaged with hot water. Thus, the PVA/KN-B/DE membrane has good application prospects in PEM fuel cells.

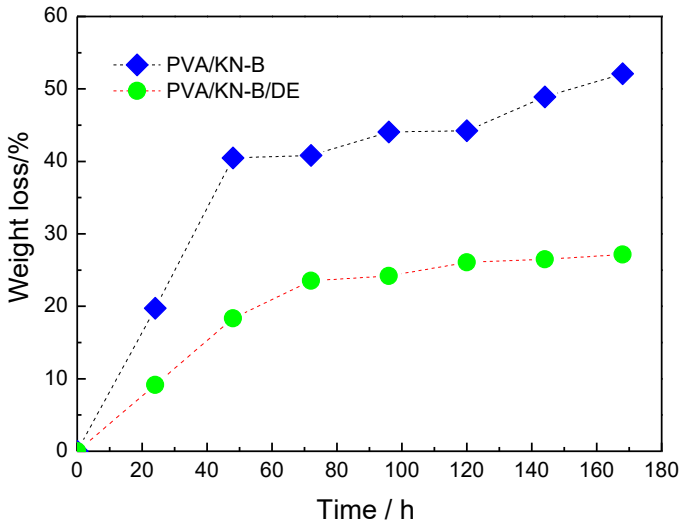

Figure 11. Time course of the synthesized membranes' weight loss in aqueous solutions of H_2O_2 (30 wt%) at room temperature

4. CONCLUSIONS

The aim of this study was to develop a novel PVA-based PEM for use in fuel cells by incorporating the reactive dye KN-B as a H^+ carrier, and the fixing agent DE as a cross-linking component. A solution-casting method combined with a soaking and baking process was carried out to synthesize the membranes, and the membranes were characterized to investigate their application performance. The FT-IR spectra, XRD graphs, XPS results and SEM images show that KN-B was successfully introduced into the PVA matrix and that a three-dimensional network structure can be constructed under the cross-linking action of DE. With the help of cross-linking, the mechanical properties of the membranes improved significantly due to the compact inner structure and the tensile strength of the membranes reached 55.6 MPa. Furthermore, the compact inner structure resulted in a decrease in WU and SR. A comparison of the films before and after crosslinking also shows that the PVA/KN-B membrane had a higher H^+ conductivity value of 0.124 S cm^{-1} at room temperature, while the PVA/KN-B/DE membrane had better anti-oxidative stability during 168 h of evaluation. Both types of membranes exhibited an increase in proton conductivity as the temperature increased from 20 ℃ to 80 ℃. The calculated E_a values, 5.49 kJ mol^{-1} for the PVA/KN-B membrane and 6.58 kJ mol^{-1} for the

PVA/KN-B/DE membrane, indicate that the Grotthuss mechanism and vehicle mechanism co-exist in the ionic transport process but with the former playing the dominant role. Due to the promising results discussed above, the prepared membranes may have a bright future in PEM fuel cells.

ACKNOWLEDGEMENTS
This work was financially supported by Open Foundation of Provincial Research Platform of Yancheng Vocational Institute of Industry Technology and Undergraduates Innovation Ability Research Foundation of Yancheng Institute of Technology, and National Natural Youth Science Foundation of China (Project Number: 51803175). The authors would like to thank to Donghua University, and Jiangsu Zhongzhan Vehicle Accessories Co., LTD for offering some chemical agents and for generous funding. All financial support is gratefully acknowledged.

References

1. Y. Wang, J. Qiao, R. Baker And J. Zhang, *Chem. Soc. Rev.,* 42 (2013) 5768.
2. D. Herranz, R. Escudero-Cid, M. Montiel, C. Palacio And P. Ocón, *Renew. Energy,* 127 (2018) 883.
3. A. Gomes And J. Filho, *Int. J. Hydrogen Energy,* 37 (2012) 6246.
4. S. Alpay, *Electrochim. Acta,* 271 (2018) 127.
5. C. González-Guisasol And A. Ribes-Greus, *Polym. Test.,* 67 (2018) 55.
6. S. Zhang And X. Lu, *Chemosphere,* 206 (2018) 777.
7. B. Hameed And Z. Ismail, *Biochem. Eng. J.,* 137 (2018) 71.
8. T. Zhou, J. Zhang, B. Ao, Y. Wei, S. Chen And J. Qiao, *Solid State Ionics,* 308 (2017) 112.
9. T. Zhou, J. Hang, J. Qiao, L. Liu, G. Jiang, J. Zhang And Y. Liu, *J. Power Sources,* 227 (2013) 291.
10. T. Zhou, J. Zhang, G. Jiang, J. Zhang And J. Qiao. *Synth. Met.,* 167 (2013) 43.
11. J. Zhang, T. Zhou, J. Qiao, Y. Liu And J. Zhang, *Electrochim. Acta,* 111 (2013) 351.
12. A. Laskar, M. Khan, F. Askari And H. Younus, *Int. J. Biol. Macromol.,* 103 (2017) 99.
13. A. Dafalla And F. Jiang, *Int. J. Hydrogen Energy,* 43 (2018) 2327.
14. T. Zhou, R. Shao, S. Chen, X. He, J. Qiao And J. Zhang, *J. Power Sources,* 293 (2015) 946.
15. S. Peighambardoust, S. Rowshanzamir And M. Amjadi, *Int. J. Hydrogen Energy,* 35 (2010) 9349.
16. H. Tomoya, M. Kazuya And U. Mitsuru, *Polymer,* 50 (2009) 5341.
17. J. Qiao, J. Fu, R. Lin, J. Ma And J. Liu, *Polymer,* 51 (2010) 4850.
18. T. Zhou, F. Song, X. He And K. Xie, *Solid State Ionics*., 282 (2015) 18.
19. J. Qiao, J. Fu, L. Liu, Y. Liu And J. Sheng, *Int. J. Hydrogen Energy,* 37 (2012) 4580.
20. M. Saadiah, D. Zhang, Y. Nagao, S. Muzakir And A. Samsudin, *Journal of Non-Crystalline Solids,* 511 (2019) 201.
21. C. Liew, S. Ramesh And A. Arof, *Int. J. Hydrogen Energy,* 39 (2014) 2953.
22. A. El-Shamy, *Prog. Org. Coat.,* 127 (2019) 252.
23. B. Baraker And B. Lobo, *Materials Today: Proceedings*, 5 (2018) 3036.
24. Z. Wang, L. Wu, J. Zhou, W. Cai, B. Shen And Z. Jiang, *J. Phys. Chem. C,* 117 (2013) 5446.
25. O. Rodríguez-Uicab, F. Avilés, P. Gonzalez-Chi, G. Canché-Escamilla, S. Duarte-Aranda, M. Yazdani-Pedram, P. Toro, F. Gamboa, M. Mazo, A. Nistal And J. Rubio, *Appl. Surf. Sci.,* 385 (2016) 379.
26. J. Li, M. Zhou, J. Lin, W. Ye, Y. Xu, J. Shen, C. Gao And B. Bruggen, *J. Membrane Sci.,* 486 (2015) 89.
27. Y. Lin, L. Wang, J. Zhou, L. Ye, H. Hu, Z. Luo And L. Zhou, *Polymer,* 162 (2019) 80.
28. M. Nasef And H. Saidi, *Appl. Surf. Sci.,* 252 (2006) 3073.
29. L. Shao, J. Li, Y. Guang, Y. Zhang, H. Zhang, X. Che And Y. Wang, *Mater. Design,* 99 (2016)235.
30. N. Ojah, D. Saikia, D. Gogoi, P. Baishya, G. Ahmed, A. Ramteke And A. Choudhury, *Appl. Surf.*

Sci., 475 (2019) 219.
31. A. Mondal, C. Cheng, Z. Yao, J. Pan, M. Hossain, M. Khan, Z. Yang, L. Wu And T. Xu, *J. Membrane Sci.,* 490 (2015) 29.
32. G. Li, J. Xie, H. Cai And J. Qiao, *Int. J. Hydrogen Energy,* 39 (2014) 2639.
33. J. Zhang, Z. Wang, Q. Wang, J. Ma, J. Cao, W. Hu And Z. Wu, *J. Membrane Sci.,* 537 (2017) 263.
34. C. Amri, M. Mudasir, D. Siswanta And R. Roto, *Int. J. Biol. Macromol.,* 82 (2016) 48.
35. J. Qiao, T. Okada And H. Ono, *Solid State Ionics,* 180 (2009) 1318.
36. M. Casciola, G. Alberti, M. Sganappa And R. Narducci, *J. Power Sources,* 162 (2006) 141.
37. H. Beydaghi, M. Javanbakht, H. Amoli, A. Badiei, Y. Khaniani, M. Ganjali, P. Norozui And M. Abdouss, *Int. J. Hydrogen Energy,* 36 (2011) 13310.
38. B. Lin, L. Qiu, J. Lu And F. Yan, *Chem. Mater.,* 22 (2010) 6718.
39. T. Zhou, X. He And K. Xie, *J. Appl. Polym. Sci.,* 133 (2016) 43019.
40. S. Elakkiya, G. Arthanareeswaran, A. Ismail, D. Das And R. Suganya, *Eur. Polym. J.,* 112 (2019) 696.
41. S. Elakkiya, G. Arthanareeswaran, K. Venkatesh And J. Kweon, *Int. J. Hydrogen Energy,* 43 (2018) 21750.
42. H. Lee, J. Han, K. Kim, J. Kim, H. Shin And J. Lee, *J. Ind. Eng. Chem.,* 74 (2019) 223.
43. K. Oh, O. Kwon, B. Son, D. Lee, S. Shanmugam, *J. Membrane Sci.,* 583 (2019) 103.
44. F. Teixeira, A. Sá, A. Teixeira And C. Rangel, *Appl. Surf. Sci*., 487 (2019) 889.
45. Q. Xu, L.Wang, C. Li, X. Wang, C. Li And Y. Geng, *Int. J. Hydrogen Energy,* 44 (2019) 15322.
46. B. Munavalli And M. Kariduraganavar, *Electrochim. Acta,* 296 (2019) 294.
47. T. Zhou, M. Wang, X. He And J. Qiao, *Journal of Materiomics,* 5 (2019) 286.
48. Z. Pan, L. An, T. Zhao And Z. Tang, *Prog. Energ. Combust.,* 66 (2018) 141.
49. R. Rudra, V. Kumar And P. Kundu, *RSC Adv.,* 101 (2015) 83436.
50. Y. Gao, F. Song, J. Qiao, S. Chen, X. Zhao And J. Zhang, *Electrochim. Acta,* 177 (2015) 201.
51. B. Wang, Y. Zhu, T. Zhou And K. Xie, *Int. J. Hydrogen Energy,* 41 (2016) 18166.
52. E. Kim, S. Lee, S. Woo, S. Park And B. Bae. *J. Power Sources,* 359 (2017) 568.
53. B. Einsla, Y. Kim, M. Hickner, Y. Hong, M. Hill, B. Pivovar And J. Mcgrath, *J. Membrane Sci.*, 255 (2005) 141.
54. F. Song, Y. Fu, Y. Gao, J. Li, J. Qiao, X. Zhou And Y. Liu, *Electrochim. Acta,* 177 (2015) 137.